© 2017. Published by The Company of Biologists Ltd | Journal of Experimental Biology (2017) 220, 2096-2107 doi:10.1242/jeb.147934

RESEARCH ARTICLE

Model-assisted measurements of suspension-feeding flow velocities

Kevin T. Du Clos*,¶, Ian T. Jones‡, Tyler J. Carrier§, Damian C. Brady and Peter A. Jumars

ABSTRACT

Benthic marine suspension feeders provide an important link between benthic and pelagic ecosystems. The strength of this link is determined by suspension-feeding rates. Many studies have measured suspension-feeding rates using indirect clearance-rate methods, which are based on the depletion of suspended particles. Direct methods that measure the flow of water itself are less common, but they can be more broadly applied because, unlike indirect methods, direct methods are not affected by properties of the cleared particles. We present pumping rates for three species of suspension feeders, the clams *Mya arenaria* and *Mercenaria mercenaria* and the tunicate *Ciona intestinalis*, measured using a direct method based on particle image velocimetry (PIV). Past uses of PIV in suspension-feeding studies have been limited by strong laser reflections that interfere with velocity measurements proximate to the siphon. We used a new approach based on fitting PIV-based velocity profile measurements to theoretical profiles from computational fluid dynamic (CFD) models, which allowed us to calculate inhalant siphon Reynolds numbers (*Re*). We used these inhalant *Re* and measurements of siphon diameters to calculate exhalant *Re*, pumping rates, and mean inlet and outlet velocities. For the three species studied, inhalant *Re* ranged from 8 to 520, and exhalant *Re* ranged from 15 to 1073. Volumetric pumping rates ranged from 1.7 to 7.4 l h^{-1} for *M. arenaria*, 0.3 to 3.6 l h^{-1} for *M. mercenaria* and 0.07 to 0.97 l h^{-1} for *C. intestinalis*. We also used CFD models based on measured pumping rates to calculate capture regions, which reveal the spatial extent of pumped water. Combining PIV data with CFD models may be a valuable approach for future suspension-feeding studies.

KEY WORDS: Suspension feeding, PIV, CFD, Fluid mechanics, Bivalve, Tunicate

INTRODUCTION

Benthic marine suspension feeders provide an important link between benthic and pelagic ecosystems. Effects of suspension-feeding activity include exerting top-down control on phytoplankton growth (e.g. Caraco et al., 2006; Cerco and Noel, 2007, 2010; Newell, 1988; Officer et al., 1982), concentrating organic matter into fecal pellets with high settling speeds, reducing turbidity (Newell and Koch, 2004), and competing with (Cloern, 1982) and grazing on (Green et al., 2003) zooplankton. In addition, many active suspension feeders, such as the bivalves *Mya arenaria* and *Mercenaria mercenaria*, support commercial fisheries, and many others, such as the tunicate *Ciona intestinalis*, are fouling organisms with negative economic impacts.

In the case of active suspension feeders – those that use pumping, rather than ambient currents, to deliver the suspended particles on which they feed (Wildish and Kristmanson, 1997) – the rates of the suspension-feeding functions listed above are ultimately controlled by the flows produced by individual suspension feeders and the interactions of these flows with each other and with ambient flows. Such flows have been quantified in various ways for more than 90 years (e.g. Galtsoff, 1926). Active suspension feeding is common among bivalves, ascidians, bryozoans, polychaetes, and burrowing and tube-dwelling crustaceans, especially those occupying moderate flow regimes. An active suspension feeder produces inhalant and exhalant flows through unfused mantle margins, a straight or U-shaped tube or burrow, or a pair of well-formed siphons such as those of our study organisms.

Exhalant siphon flows (jets flows) are well studied in fluid mechanics – largely because of their relevance to aerospace engineering (Karagozian, 2014). In marine systems, bivalve exhalant jets have been shown to produce shear that enhances mixing in benthic boundary layers, which likely helps to limit local depletion of seston (Lassen et al., 2006), and physical siphon analogs have been used to study interactions between jet flows and boundary-layer flows (Crimaldi et al., 2007; Monismith et al., 1990; O'Riordan et al., 1993, 1995).

Inhalant siphon flows, in contrast, have not received as much attention, either from a fluid mechanical or a marine ecological perspective. They are arguably more important than jet flows for suspension feeding, however, because they define the spatial extent of the water pumped by a suspension feeder. These flows thus set an upper limit on the suspension feeder's growth rate and its influence on seston concentration, and determine the chemical cues to which it has access. From a marine ecology perspective, inhalant siphon flows have been recognized as triggers for copepod escape reactions (Kiørboe et al., 1999; Fields and Yen, 1996, 1997; Fields, 2010; Fields et al., 2012) and for their roles in the cannibalistic capture of larvae by the cockle *Cerastoderma edule* (André et al., 1993). Detailed studies of inhalant flow are likely to improve parameterizations in ecological models that include suspension feeding (e.g. Cerco and Noel, 2010). Specifically, these studies could be used to identify flow conditions and animal densities at which interactions between neighbors become significant and to scale individual suspension-feeding rates up to population scales. Because inhalant flows are convergent, velocities drop off rapidly with distance from the siphon inlet, often falling below measurement thresholds at short distances from the inlet. This property of inhalant flows makes them more difficult to study than jet flows.

Darling Marine Center, School of Marine Sciences, University of Maine, 193 Clarks Cove Road, Walpole, ME 04573-3307, USA.
*Present address: Department of Integrative Biology, University of South Florida, 4202 East Fowler Ave, Tampa, FL 33620, USA. ‡Present address: Biology Department, Woods Hole Oceanographic Institution, 266 Woods Hole Road, Woods Hole, MA 02543-1535, USA. §Present address: Department of Biological Sciences, University of North Carolina at Charlotte, 9201 University City Blvd, Charlotte, NC 28223-00001, USA.

¶Author for correspondence (duclos@usf.edu)

K.T.D., 0000-0002-3017-7777

Received 9 August 2016; Accepted 21 March 2017

Journal of Experimental Biology

Journal of Experimental Biology (2017) 220, 2096-2107 doi:10.1242/jeb.147934

Methods for measuring suspension-feeding activity can be divided into two groups: 'indirect' methods based on the depletion of suspended particles and 'direct' methods based on water flow (Riisgård, 2001). The most common indirect method is to take repeated water samples from a tank containing suspension feeders, quantify the concentration of particles in each sample, and fit a function to describe the relationship between particle concentration and time. Indirect clearance-rate measurements are useful for comparing feeding activity between species and under varying conditions within a study, but results depend on the properties of the particles used (Møhlenberg and Riisgård, 1978; Rosa et al., 2017). They can also be affected by variations in experimental conditions because of local depletion of particles and flow effects of nearby tank walls (Riisgård, 2001).

Several direct methods have been developed. Particle-based methods – particle imaging velocimetry (PIV) and particle tracking velocimetry (PTV) – have two advantages over most other direct methods. They are non-invasive, and they produce spatially and temporally resolved velocity data in addition to flow rates. Troost et al. (2009) used PIV and PTV to measure inhalant velocities produced by three bivalve species; they modeled rather than measured exhalant velocities because exhalant water was depleted of particles. Frank et al. (2008) measured exhalant velocities for four bivalve species and the tunicate *Styela clava* by performing PIV with small particles (~2 µm) that were inefficiently retained. They found that exhalant velocities were positively correlated with clearance rates. Inhalant velocity measurements were not included. Nishizaki and Ackerman (2017) used PIV to characterize exhalant flow structures produced by dreissenid mussels. In another PIV application, Delavan and Webster (2012) found an increase in variance in *Mercenaria mercenaria* exhalant siphon velocities in the presence of a predator. André et al. (1993) used PTV to study cannibalism on larvae by *Cerastoderma edule*. Stamhuis and colleagues (Stamhuis et al., 2002; Stamhuis, 2006) discussed suspension-feeding flows as part of two broader reviews of applications of PIV to biological problems.

As others have noted (Frank et al., 2008; Troost et al., 2009), one limitation of PIV is that laser light reflected by the animal often makes it impossible to obtain accurate velocity measurements immediately adjacent to a suspension feeder's siphon. Quantifying velocity at the siphon inlet is crucial, however, for calculating pumping rates. Reconstructing the proximate flow field based on the available data requires a model of the flow field's structure. Profiles of velocity, starting at the center of the siphon inlet and extending away from the siphon along its axis, are commonly used. These profiles have been modeled using empirical (Troost et al., 2009), analytical (Kiørboe et al., 1999) and numerical (Jumars, 2013) approaches, but only the numerical approach is able to accurately represent the flow near the siphon inlet. Empirical models, such as exponential fits (Troost et al., 2009), are reasonable approximations of axial profiles when the entire profile is available. Inlet velocities cannot reliably be extrapolated from partial profiles, however, because velocity increases so rapidly as distance to the siphon inlet decreases. Small errors in velocity measurements made at intermediate distances from the siphon inlet thus propagate to create large errors in velocity calculations at the siphon inlet. Analytical models for flow into a siphon are generally oversimplified, the most common simplification being the point-sink model. Jumars (2013) produced numerical computational fluid dynamics (CFD) models of inhalant siphon flows and demonstrated that the point-sink model, despite predicting realistic velocities in the far field, rapidly diverges from the true velocity fields on approaching the siphon inlet. In fact, the point-sink model predicts an infinite velocity at the siphon inlet. We used CFD models similar to those used by Jumars (2013) to interpret velocity fields produced in our PIV experiments.

The key dimensionless parameter for describing flow into an inhalant siphon is the inhalant siphon Reynolds number:

$$Re_{\mathrm{in}} = \frac{\overline{W}_{\mathrm{in}} D_{\mathrm{in}}}{\nu}, \quad (1)$$

where $\bar{W}_{\mathrm{in}}$ is the velocity averaged across the siphon inlet, D_{in} is the inner diameter of the inhalant siphon and ν is the kinematic viscosity of the fluid, which equals the dynamic viscosity (µ) divided by the density (ρ). Exhalant siphon Reynolds number (Re_{ex}) can be found in the same way by substituting exhalant siphon values for velocity ($\bar{W}_{\mathrm{ex}}$) and diameter (D_{ex}). Despite the central importance of *Re* in determining flow dynamics (Batchelor, 1967, pp. 211–215), most reported measurements of suspension feeding rate include no explicit measurements of siphon inner diameter (Jumars, 2013). Our analysis emphasizes the importance of *Re* and its utility for comparing suspension-feeding flows.

In this study, we used PIV to measure velocity fields produced by the inhalant siphons of three species of active suspension feeders, the bivalves *Mya arenaria* and *Mercenaria mercenaria* and the tunicate *Ciona intestinalis*. We chose these species because we expected them to pump over a wide range of Re_{in} and because they are common and well studied, enabling us to compare our results with published measurements. As in the previously cited PIV studies of inhalant siphon velocity, we were unable to measure velocities immediately adjacent to the siphon inlet. We therefore used CFD models of inhalant siphon flows based on those developed by Jumars (2013) to calculate Re_{in}. We then used these Re_{in} values and measurements of siphon diameter to calculate mean inlet and outlet velocities, pumping rates and Re_{ex}.

MATERIALS AND METHODS

Animals

Mya arenaria Linnaeus 1758 (n=9) and *Mercenaria mercenaria* Linnaeus 1758 (n=7) clams were obtained locally, either from seafood suppliers or intertidal sand beaches, and maintained in the flowing seawater facility at the University of Maine's Darling Marine Center (Walpole, ME, USA). *Ciona intestinalis* (Linnaeus 1767) tunicates (n=6) were carefully detached from tank surfaces on which their larvae had naturally settled in the same flowing seawater facility. Individuals were chosen to provide a range of sizes for comparison (Table 1). One *C. intestinalis* individual was excluded from analysis because of poor velocity field data.

Table 1. Ranges of measurements of experimental animals

	Mya arenaria	*Mercenaria mercenaria*	*Ciona intestinalis*
Total WW (g)	2.54–34.09	26.54–69.36	5.79–15.90
Total DW (g)	0.98–12.11	16.8–45.2	0.28–1.04
Flesh AFDW (g)	0.06–1.03	0.57–1.04	0.20–0.84
Shell/body *L* (mm)	28.9–66.5	44.5–62.8	65.0–91.5
Shell width (mm)	16.9–37.1	36.4–55.5	
D_{in} (mm)	2.3–4.7	1.6–3.7	7.0–10.3
D_{ex} (mm)	1.4–3.0	1.2–2.5	4.0–4.9
n	9	7	6

WW, wet weight; DW, dry weight; AFDW, ash-free dry weight; *L*, length; D_{in}, inhalant diameter; D_{ex}, exhalant diameter.

Journal of Experimental Biology

Journal of Experimental Biology (2017) 220, 2096-2107 doi:10.1242/jeb.147934

Particle image velocimetry

Stereoscopic PIV was performed using a commercial system (LaVision, Goettingen, Germany) with a pulsed ND:YAG laser with an emission wavelength of 532 nm (New Wave Research, Fremont, CA, USA) and two Imager Intense cameras each with a resolution of 1376×1040 pixels (LaVision). Experiments were performed in a 30×30×30 cm tank filled to 27–28 cm with filtered seawater. The water was seeded with hollow glass spheres (diameter=9–13 µm, ρ=1.10±0.05 g cm^{-3}; LaVision) and maintained at a temperature of 17–19°C and practical salinity of ∼30–32. This range of temperatures and salinities corresponds to a kinematic viscosity of $\nu \approx 1.1\times10^{-6}$ m^2 s^{-1} (Nayar et al., 2016; Sharqawy et al., 2010), the value used for all calculations. Approximately 2×10^6 *Tetraselmis chuii* cells were added to the tank at the beginning of each experiment to induce feeding. Each experiment lasted <10 h.

For each experiment with *M. arenaria* or *M. mercenaria*, an individual was buried in a 190×100 mm (diameter×depth) glass dish filled with playground sand with the ends of its siphons protruding above the surface. The clam was oriented with its sagittal plane perpendicular to the image plane and its inhalant siphon closest to the camera, with the laser sheet bisecting the inhalant siphon. A thin layer of black sand was added at the sediment–water interface to reduce reflections. Images were captured in double-frame mode with the duration between frames ('dt') chosen to optimize particle shift (approximately 10 pixels per frame near the inhalant siphon) for an individual clam: 25–80 ms for *M. arenaria* and 40–99 ms for *M. mercenaria*. Image pairs were captured at a recording rate of 2.5 Hz. For experiments with *C. intestinalis*, a tunicate was arranged with its base buried in sand. *Ciona intestinalis* produced much lower flow velocities than the clams, so images were recorded in single-frame mode with a recording rate of 3.5 Hz. PIV velocity data are publicly available through the Biological and Chemical Oceanography Data Management Office (bco-dmo.org, accession numbers 655604 and 655656).

For each individual, 10 sequences were analyzed. Each sequence lasted 40 s and consisted of 100 sequential image pairs for the clams and 140 sequential images for *C. intestinalis*. LaVision's DaVis software was used to calculate vector fields from particle images. Images were first preprocessed by applying a time-averaged minimum filter to minimize noise and masking out sediment and the animal's body using a combination of a manually drawn mask and one based on intensity. Vector fields were then calculated using one pass with 64×64 pixel (50% overlap) interrogation windows followed by four passes with 32×32 pixel (75% overlap) windows. Sequences of vector fields were time averaged, yielding 10 velocity fields per animal (Fig. 1). Only sequences in which the animal was actively pumping with its siphons fully open were used, so our results represent maximal – rather than average – pumping rates.

Axial and radial velocity profiles

PIV-derived velocity fields were imported into MATLAB (MathWorks, Natick, MA, USA) for analysis. Velocity profiles were extracted from the time-averaged velocity field for each PIV sequence (Figs 1 and 2). Our CFD models are axisymmetric, so we also assigned cylindrical coordinates to our PIV-derived velocity fields. The origin is defined as the center of the siphon inlet (Fig. 2, schematics). The *z*-axis is aligned with the symmetry axis and is perpendicular to the siphon inlet. The *r*-axis is perpendicular to the symmetry axis and parallel to the siphon inlet. The *r* and *z* components of velocity are *u* and *w*, respectively, and *v* corresponds to out-of-plane velocities, which are 0 in the models. The origin and

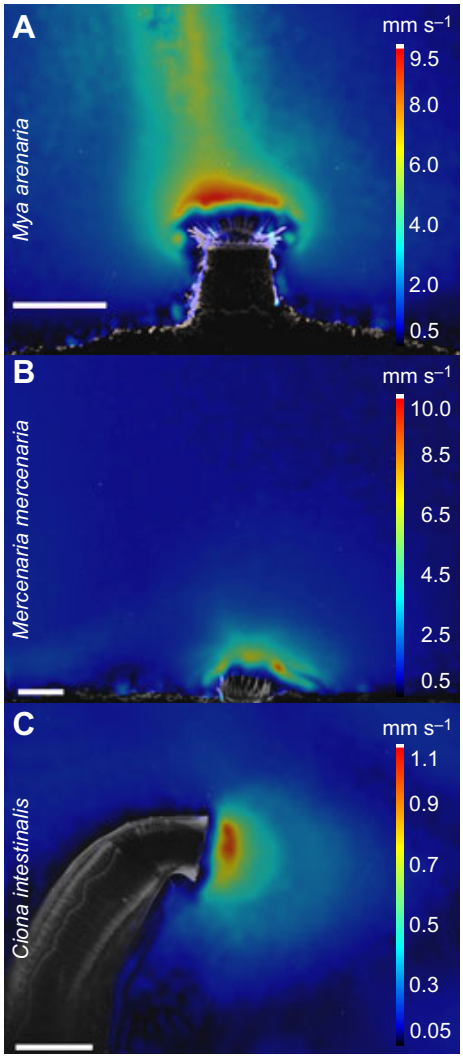

Fig. 1. Velocity magnitude plots from example time-averaged 40 s sequences for the three study species. (A) *Mya arenaria*, (B) *Mercenaria mercenaria* and (C) *Ciona intestinalis*. Note the influence of the exhalant jet above and to the left of the siphon in A.

rotation of the axes for each sequence were determined based on PIV images. A velocity profile, hereafter referred to simply as a profile, represents the velocity along a transect drawn along or at an angle to the *z*-axis (axial) or parallel to the *r*-axis (radial).

For each sequence, an axial profile was taken along a 30 mm transect beginning at the inhalant siphon center (Fig. 2A). To reduce the influence of the exhalant flow, calculations were based on profiles of 'inward' velocity, i.e. the component of the velocity vector directed toward the siphon center. Inward velocity was calculated by a scalar projection of the velocity vector at each point onto the profile (Fig. 2A). The angle of the profile was chosen by selecting the profile with the maximum inward velocity magnitude within 10 deg of the *z*-axis. For some sequences, the exhalant siphon had a strong influence on the axial profile, so the profile was taken at ±30 or ±60 deg from the *z*-axis, and the profile was fitted to CFD profiles taken at the same angle. For a convergent flow, the highest inhalant velocities outside the siphon are found closest to the inlet. Because of reflections, we were unable to accurately measure velocities within a radius of ∼4–6 mm of the inhalant siphon center, so velocity measurements in this region are unrealistically low (Fig. 2A).

Journal of Experimental Biology (2017) 220, 2096-2107 doi:10.1242/jeb.147934

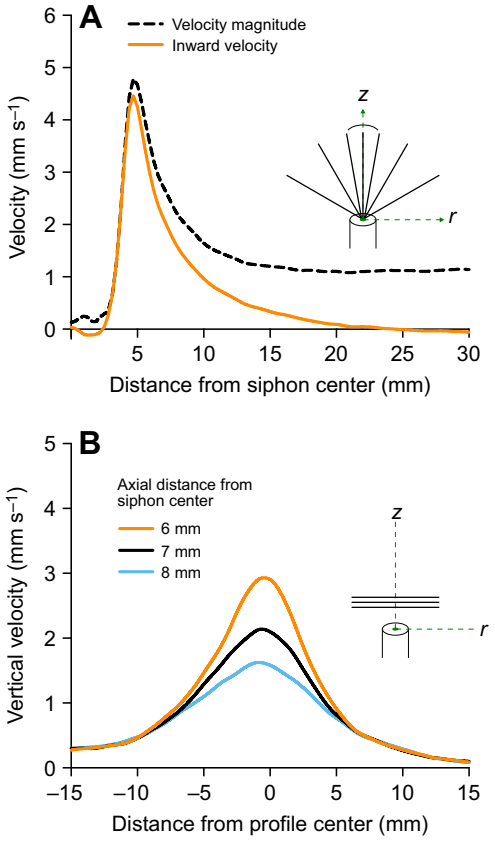

Fig. 2. Example velocity profiles for *Mya arenaria* from a time-averaged 40 s sequence. Schematics show the locations of each type of profile with respect to the siphon. (A) Axial profiles of velocity magnitude (dashed black line) and inward velocity (orange line), the component of velocity directed toward the siphon center. (B) Radial profiles of vertical velocity centered at 6 mm (orange), 7 mm (black) and 8 mm (blue) from the siphon center.

Three radial profiles of vertical velocity were taken along transects perpendicular to and centered on the *z*-axis – one each centered at 6, 7 and 8 mm from the origin (Figs 1B, 2B). Analogously to the use of inward velocity for axial profiles, the vertical velocity component *w* was used to restrict the influence of the exhalant siphon. The profile was split at the *z*-axis, and the mean of the two halves was used for further calculations. In some cases, the influence of exhalant flow rendered one half of the profile unusable, so the remaining half was used. All processing code is available from the corresponding author upon request. As a validation of the method, values of Re_{in} calculated from axial and radial profiles were compared by fitting a linear regression between the axial value and the median of the three radial values for each sequence.

Numerical models

The PIV-derived profiles described above were fitted to equivalent profiles taken from CFD models to calculate Re_{in} for each image sequence. The CFD model geometry consists of an axisymmetric inhalant siphon drawing from a large, hemispherical domain. The models are similar to the 'capillary' model described by Jumars (2013) but with a shorter capillary length (3 mm for the clams and 10 mm for *C. intestinalis*) and an inner diameter matched to that of the experimental animal. The fluid was assigned a kinematic viscosity of $\nu=1.1\times10^{-6}$ m^2 s^{-1}. Simulations were carried out in COMSOL Multiphysics (COMSOL, Burlington, MA, USA), using the PARDISO solver and the BDF time-stepping method. Initial model simulations were performed to ensure that the profiles were mesh independent and uninfluenced by the presence of domain walls. The model was run over a range of Re_{in} values and inhalant siphon diameters. A study by True and Crimaldi (2017) showed that similar models perform well against experimental data from a physical siphon model with a known flow rate.

We define a capture region as the spatial extent of the fluid drawn into an inhalant siphon over a given pumping duration. Capture-region boundaries were calculated using the Particle Tracing module of COMSOL by placing 20,000 passive Lagrangian tracers across the siphon inlet and advecting them backwards in time using the previously calculated time-dependent velocity fields. We calculated capture-region bounds for each species based on the individual with the highest Re_{in}. We also calculated maximum capture region extents in the *r* direction for each species based on the individuals with the smallest and largest Re_{in}. These calculations are for the case where water motion is provided only by animal pumping, thus maximizing the potential effects of nearest-neighbor interactions.

We compared the extent of capture regions with estimates of mean nearest-neighbor distances (r_n) for each species based on assumptions of random and uniform distributions. For a randomly distributed population, r_n can be calculated using the equation:

$$r_n = \frac{1}{2\sqrt{p}}, \quad (2)$$

where p is population density; multiplying this distance by 2.15 gives the r_n for a uniformly distributed population (Clark and Evans, 1954).

Reynolds number calculations

For each PIV sequence, we fitted axial and radial profiles to their equivalent CFD profiles over a range of Re_{in} and maximized R^2 between PIV and CFD profiles to select a value for Re_{in}. Those values for which $R^2<0.3$ were excluded from further analyses. This cut-off was chosen by visually inspecting fits between PIV and CFD profiles. We also performed a sensitivity analysis using the same fitting method to test how errors in measuring siphon position and angle are likely to affect Re_{in} calculations (Appendix).

Based on the Re_{in} values, we calculated volumetric flow rate (Q) and mean velocity across the siphon inlet ($\overline{W}_{in}$), using the following equations (in SI units):

$$Q = \frac{1}{4}\pi\nu Re_{in} D_{in}, \quad (3)$$

$$\overline{W}_{in} = \frac{Re_{in}\nu}{D_{in}}, \quad (4)$$

where ν is kinematic viscosity and D_{in} is inhalant siphon diameter. Volumetric flow rates through the inhalant and exhalant siphons must be equal, so Re_{ex} was calculated by equating the right side of Eqn 3 for inhalant and exhalant Re and D. Simplifying and rearranging the resulting equation gives:

$$Re_{ex} = Re_{in}\frac{D_{in}}{D_{ex}}. \quad (5)$$

In words, Re_{ex} is Re_{in} multiplied by the ratio of inhalant to exhalant siphon diameter. Mean outlet velocity can be found by rewriting Eqn 4 in terms of exhalant quantities or using the equation:

$$\overline{W}_{ex} = \overline{W}_{in} \times \left(\frac{D_{ex}}{D_{in}}\right)^2, \quad (6)$$

Journal of Experimental Biology (2017) 220, 2096-2107 doi:10.1242/jeb.147934

from which we see that the ratio of exhalant to inhalant velocity is dependent on the square of exhalant to inhalant siphon diameter.

Allometric relationships

After each experiment, inhalant and exhalant siphons were photographed with a scale, and lengths of the major and minor axes of the inner perimeters of inhalant and exhalant siphon openings were measured from the photographs. These measurements were used to calculate equivalent circular diameters – the diameter of a circle with the same area as the ellipse with the measured major and minor axes – on which calculations and model parameterizations were based. Shell length and width were also measured for the clams, and body length was measured for *C. intestinalis*. Blotted wet weights (WW), dry weights (DW) and ash-free dry weights (AFDW) were obtained after blotting the animal dry with a paper towel, oven drying for at least 48 h at 60°C, and combusting overnight at 500°C, respectively. For the clams, WW and DW include shells, but AFDW does not. To facilitate comparison with the literature, AFDW was used as the metric of weight for clams, and WW was used for *C. intestinalis*. Where possible, allometric relationships were determined based on power-law fits between measured quantities.

Statistical analyses

Statistical analyses were performed using GraphPad Prism (GraphPad Software, La Jolla, CA, USA). In order to produce 10 useable image sequences for each animal, multiple sequences were often taken within a relatively short period. To avoid pseudoreplication due to autocorrelation in time, we therefore treated an individual animal, rather than a sequence, as a replicate. Because we fitted our experimental profiles to profiles from CFD models with a necessarily discontinuous range of Re_{in}, we used nonparameteric methods. After excluding Re_{in} values for which $R^2<0.3$, a final value of Re_{in} for each sequence was chosen by taking the median of the values from the axial profile and the three radial profiles.

RESULTS

Allometric relationships

Power-law functions were used to examine relationships between length, weight and inhalant and exhalant siphon diameters (Fig. 3). Length and weight were positively correlated for all three species (Fig. 3A,B). Based on a linear regression forced through the origin, DW for *C. intestinalis* were approximately 6% of WW (R^2=0.68, not shown), similar to the 5% reported by Randløv and Riisgård (1979). DW was not available for one *C. intestinalis* individual due to improper drying.

Length and inhalant siphon inner diameter were positively correlated for all three species (Fig. 3C,D), but R^2 values were low for *M. mercenaria* (R^2=0.12) and *C. intestinalis* (R^2=0.15).

The ratio of inhalant to exhalant diameter was calculated for each species by performing a linear regression forced through the origin (not shown). Inhalant to exhalant diameter ratios were approximately 1.6 for *M. arenaria* (R^2=0.35), 1.4 for *M. mercenaria* (R^2=0.36) and 1.9 for *C. intestinalis* (R^2=0.23).

Reynolds numbers

For *M. arenaria*, all of the 360 calculated Re_{in} values (one axial and three radial for each sequence) had associated R^2 values greater than 0.3, so all values were used. Radial profiles at higher Re_{in} tended to slightly underestimate Re_{in} compared with their axial equivalents: $Re_{rad}=0.74\times Re_{ax}+56$ (R^2=0.83; Fig. S1A). For *M. mercenaria*, 39 out

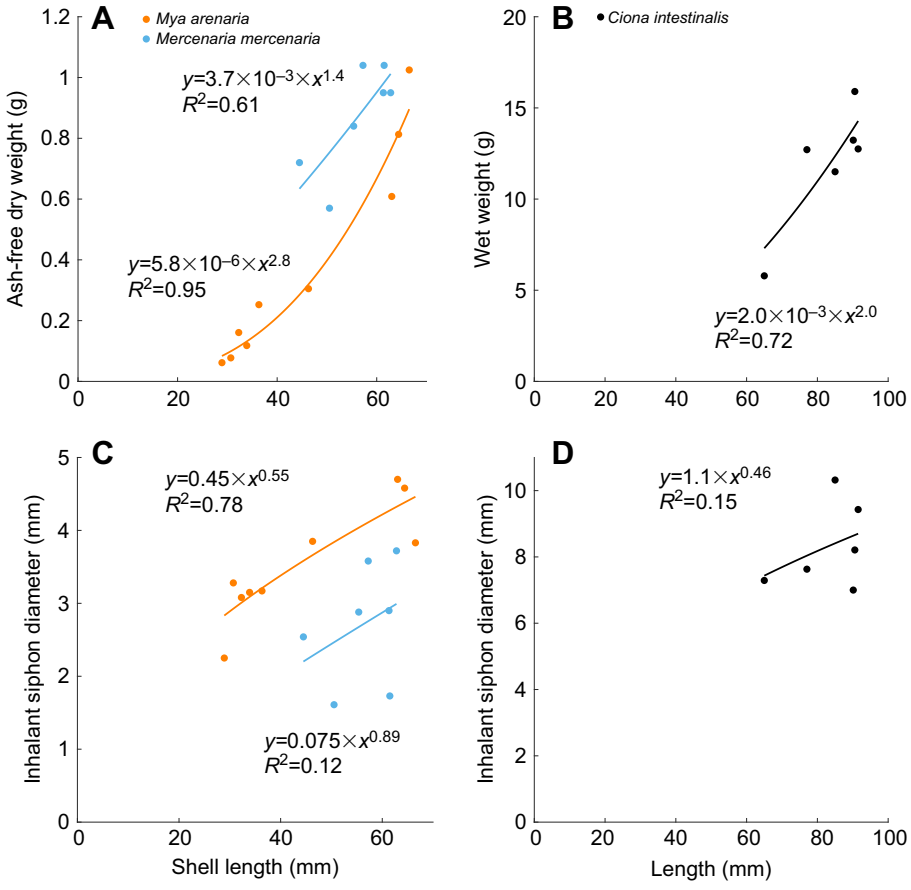

Fig. 3. Allometric relationships for *Mya arenaria* (*n*=9), *Mercenaria mercenaria* (*n*=7) and *Ciona intestinalis* (*n*=6). (A,B) Weight plotted against shell or organism length. (C,D) Inhalant siphon diameter (D_{in}) plotted against shell or body length. Lines indicate power law fits.

Journal of Experimental Biology

Journal of Experimental Biology (2017) 220, 2096-2107 doi:10.1242/jeb.147934

of 280 Re_{in} values had R^2<0.3 and were excluded. As for *M. arenaria*, radial profiles at higher Re_{in} in *M. mercenaria* tended to produce lower values than their axial equivalents: Re_{rad}=0.8×Re_{ax}+41 (R^2=0.69; Fig. S1B). For *C. intestinalis*, 20 out of 270 Re_{in} values were excluded. Axial and radial values agreed well: Re_{rad}=1.0×Re_{ax}–0.8 for *C. intestinalis* (R^2=0.76; Fig. S1C). Subsequent analyses used the median of the axial and the three radial Re_{in} values.

Re_{in} appeared to increase with weight for all three species (Fig. 4A,B), but R^2 values were low for *M. mercenaria* (R^2=0.09) and *C. intestinalis* (R^2=0.02). Median Re_{in} for individuals ranged from 179 to 520 for *M. arenaria* (n=9), 28 to 341 for *M. mercenaria* (n=7) and 8 to 33 for *C. intestinalis* (n=6; Fig. 4A,B).

Exhalant Reynolds numbers Re_{ex} (not shown) were calculated from Re_{in} based on ratios of inhalant to exhalant siphon diameter for each individual (Eqn 5). Median Re_{ex} ranged from 308 to 1073 for *M. arenaria*, 49 to 606 for *M. mercenaria* and 15 to 76 for *C. intestinalis*.

Mean inlet and outlet velocities and pumping rates

Mean inlet ($\bar{W}_{in}$) and outlet ($\bar{W}_{ex}$) velocities and pumping rates (Q) were calculated from Re_{in} and inhalant siphon diameters (Eqns 3,4,6). Median $\bar{W}_{in}$ for individuals ranged from 63 to 125 mm s^{-1} for *M. arenaria*, 8.4 to 147 mm s^{-1} for *M. mercenaria* and 0.4 to 3.8 mm s^{-1} for *C. intestinalis* (Fig. 4C,D). For all three species, the Akaike information criterion (AIC) was smaller for a linear model with slope constrained to 0 than for one with an unconstrained slope, suggesting that $\bar{W}_{in}$ was not correlated with AFDW, so fits are not shown. Median outlet velocities ranged from 153 to 532 mm s^{-1} for *M. arenaria*, 25 to 349 mm s^{-1} for *M. mercenaria* and 1 to 20 mm s^{-1} for *C. intestinalis*.

Median pumping rates (Q) ranged from 1.7 to 7.4 l h^{-1} for *M. arenaria*, 0.3 to 3.6 l h^{-1} for *M. mercenaria* and 0.1 to 1.0 l h^{-1} for *C. intestinalis* (Fig. 4E,F). Pumping rate was positively correlated with weight for *M. arenaria* and *M. mercenaria*, but not for *C. intestinalis* (R^2=0.03).

Capture regions

A capture region reveals the spatial distribution of water pumped by an inhalant siphon. Of the three species studied, *M. arenaria* had the largest capture regions for a given pumping duration, and *C. intestinalis* had the smallest as expected based on their Re_{in} values (Fig. 5). To examine possible interactions between the

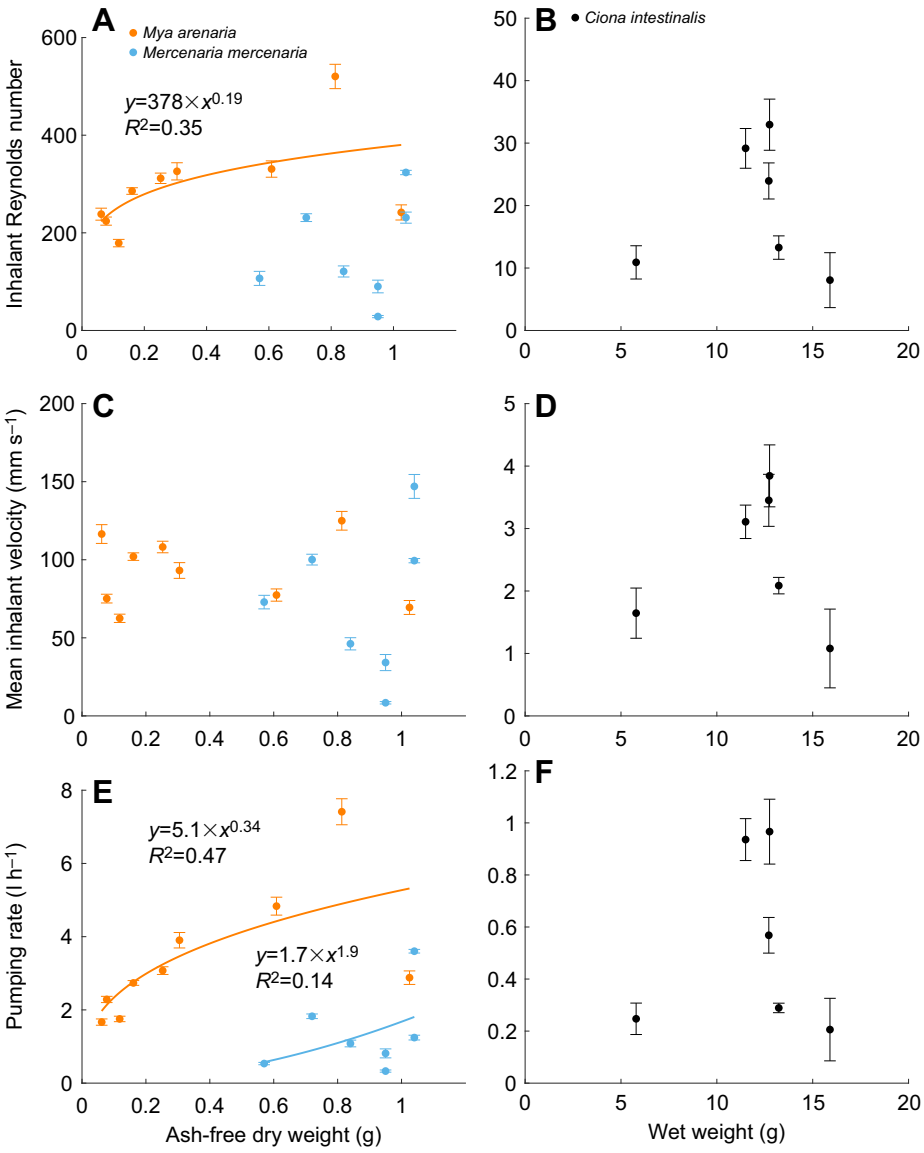

Fig. 4. Relationships between suspension-feeding parameters and weight. Individual medians and interquartile ranges of (A,B) inhalant Reynolds number Re_{in} (C,D) mean inlet velocity and (E,F) pumping rate plotted against weight for *Mya arenaria* (n=9), *Mercenaria mercenaria* (n=7) and *Ciona intestinalis* (n=6). Lines indicate power law fits. Fits with R^2<0.1 are not shown.

Journal of Experimental Biology (2017) 220, 2096-2107 doi:10.1242/jeb.147934

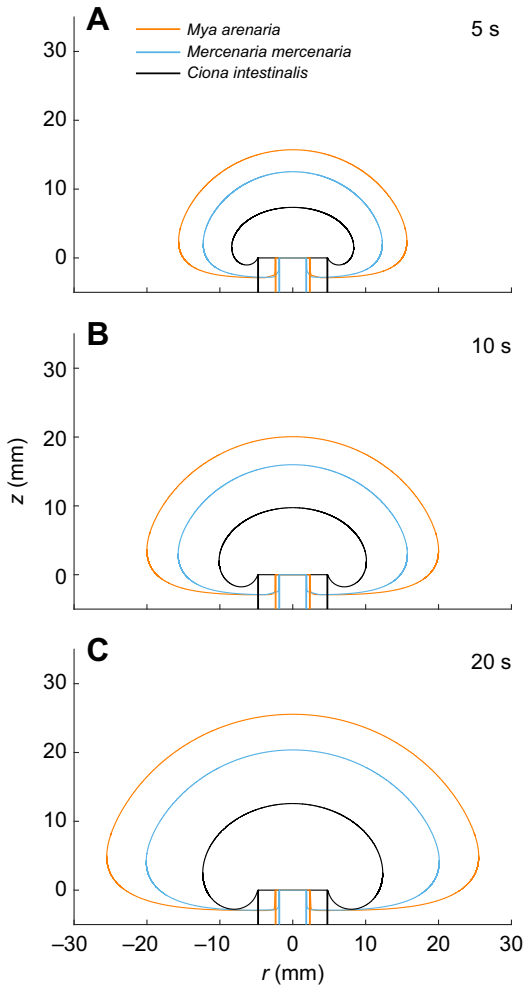

Fig. 5. Capture region outlines for each species based on the individual with the highest median Re_{in}: *Mya arenaria* (Re_{in}=520, D_{in}=4.6 mm), *Mercenaria mercenaria* (Re_{in}=340, D_{in}=3.6 mm) and *Ciona intestinalis* (Re_{in}=33, D_{in}=9.4 mm). Three pumping durations are shown: (A) 5 s, (B) 10 s and (C) 20 s.

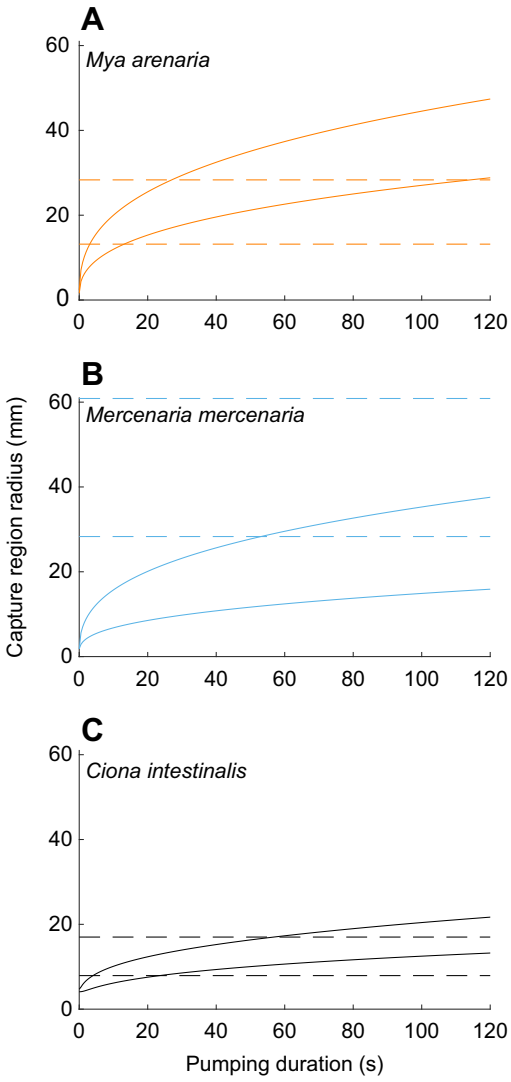

Fig. 6. Maximum capture region radius plotted against pumping duration for each species based on the individuals with the lowest and highest median Re_{in}. (A) *Mya arenaria* (Re_{in}=180, 520; D_{in}=3.2, 4.6 mm), (B) *Mercenaria mercenaria* (Re_{in}=30, 340; D_{in}=3.7, 3.6 mm) and (C) *Ciona intestinalis* (Re_{in}=8, 33; D_{in}=8.2, 9.4 mm). Dashed lines indicate half nearest neighbor distance estimates, based on densities from (A) Commito (1982), (B) Murphy (1985) and (C) Svane (1983). The top and bottom lines are calculated based on assumptions of random and uniform population distribution, respectively.

inhalant flows of neighboring animals, we compared the radial extent of capture regions over 120 s to estimates of half nearest-neighbor distance (r_n) based on the highest population densities we found in the literature: 360 m^{-2} for *M. arenaria* (Commito, 1982), 78 m^{-2} for *M. mercenaria* (Murphy, 1985) and 1000 m^{-2} for *C. intestinalis* (Svane, 1983).

We define a capture region interaction time (T_i) based on the pumping duration required for capture region radius to reach r_n divided by two – i.e. the time for adjacent capture regions to overlap (Fig. 6). For *M. arenaria* individuals with the lowest and highest Re_{in}, T_i=3.5 and 14 s for a uniform distribution and 27 and 115 s for a random distribution. For *C. intestinalis*, T_i=4.5 and 24 s for a uniform distribution and 57 s for a high Re_{in} *C. intestinalis* in a random distribution. For the high Re_{in} *M. mercenaria* in a random distribution, T_i=55 s.

DISCUSSION

Reynolds numbers and pumping rates

As predicted, the suspension-feeding flows produced by the three experimental species covered a wide range of Re_{in}, from 8 to 520 for inhalant flows and 15 to 1073 for exhalant flows. All of these Re_{in} are below 2000 – the approximate turbulence threshold for pipe flow (Reynolds, 1883; Avila et al., 2011). Gust and Harrison (1981) found Re_{in} close to the turbulent transition for pumping by burrowing shrimp and suggested that animals are unlikely to regularly pump at Re_{in} above the turbulence threshold. The energetic costs associated with pumping at high internal *Re* will likely be higher because pressure drop scales linearly with pumping rate for laminar pipe flow and with pumping rate squared for turbulent pipe flow (Wilkes, 1999, p. 115).

Reported suspension-feeding rates from the literature for *M. arenaria*, *M. mercenaria* and *C. intestinalis* vary greatly (Table 2). Direct measurements of suspension-feeding rates – such as those made using PIV – are less common than indirect measurements in the literature. Pumping rates (Q) from direct methods are related to clearance rates (C) by the filtration efficiency (E), the proportion of particles captured: $C=E\times Q$. Pumping rates cannot be directly

Journal of Experimental Biology (2017) 220, 2096-2107 doi:10.1242/jeb.147934

Table 2. Comparison of pumping rates from this study to suspension-feeding rates from the literature

Reference	Method type	*C* or *Q* (l h^{-1})	*L* (mm)	*W* (g)	Temperature (°C)	*N*
Mya arenaria						
Present study	Direct: PIV	1.7–7.4	28.9–66.5	0.06–1.03 AFDW	17–19	9
Foster-Smith, 1978	Direct: pressure-based	0.2–0.75	80		12–14	5
Riisgård and Seerup, 2003	Indirect: *E*=1	1.2–3.8	21–45	0.20–2.23 DW	11	5
Jørgensen and Riisgård, 1988	Indirect: *E*=1	2.6–6.7	58–67	0.87–2.11 DW	12	6
Allen, 1962	Indirect	0.6–1.3	57–82		17–18	6
Shumway et al., 1985	indirect	0.44		0.748 DW	12	1
Shumway and Cucci, 1987	Indirect	0.98		0.694 DW		1
Mercenaria mercenaria						
Present study	Direct: PIV	0.3–3.6	44.5–62.8	0.57–1.04 AFDW	17–19	7
Coughlan and Ansell, 1964	Direct: dye uptake	0.9–10.0	27.4–83.5	0.36–4.81 DW	18–20	14
Hamwi and Haskin, 1969	Direct: dye uptake	1.5–10.2			24	17
Cerrato et al., 2004	Indirect	0.60–1.69	40±3 (SD)		21	6
Ciona intestinalis						
This study	Direct: PIV	0.1–1.0	65.0–91.5	0.28–1.04 DW[a]	17–19	6
Goldberg et al., 1951	Direct: invasive	~2		25 WW		1
Kustin et al., 1974	Direct: invasive	0.0078–0.149		1.3–3.0 WW	16	8
	Direct: dye uptake	0.005–0.140		1.5–2.4 WW	16	12
	Indirect	0.011–0.555		1.1–3.0 WW	16	16
Fiala-Médioni, 1978	Direct: hot-film anemometry	1.084, 1.495	75, 65	0.328, 0.334 DW	15	2
	Indirect	0.802, 1.104	75, 65	0.328, 0.334 DW	15	2
Randløv and Riisgård, 1979	Indirect: *E*=1	0.10–1.41		0.003–0.318 DW	10	10
Petersen and Riisgård, 1992	Indirect: *E*=1	0.09–2.38		0.002–1.12 DW	15	26
Petersen and Svane, 2002	Indirect: *E*=1	0.3–2.9		0.026–0.142 DW	15	8

Direct methods produce pumping rates (*Q*), and indirect methods produce clearance rates (*C*). Clearance rate measurements for which 100% efficiency is assumed (*C*=*Q*) are denoted by *E*=1. Significant figures are as reported.
[a]5.79–15.90 g WW.

compared with clearance rates unless filtration efficiencies are reported as well. In general, clearance rates should be lower than pumping rates under the same conditions, but some direct methods appear to produce anomalously low rates. Methods in which a tube is inserted into the animal's siphon or the animal is otherwise constrained, which we will refer to as invasive direct methods, appear to be particularly prone to produce low pumping rates (Riisgård, 2001). Furthermore, if clearance-rate experiments use particles large enough to be retained with 100% efficiency, pumping rates and clearance rates will be equal (Møhlenberg and Riisgård, 1978). As expected, our results agree most closely with previous results based on non-invasive, direct methods or indirect methods where *E*=1.

Allometric scaling

Relationships between body size and *C* or *Q* are generally expressed in terms of power-law functions of the form $Q=a\times W^{b}$ or $Q=c\times L^{d}$, where *a*, *b*, *c* and *d* are fit parameters, and *W* and *L* are body weights and shell or body lengths, respectively. Riisgård and Seerup (2003) suggested that in general, *Q* should be proportional to length squared for bivalves because gill area should scale with shell length squared, and *Q* should be directly proportional to gill area, and therefore they suggest an exponent of *b*=2/3 for the relationship between *Q* and *W*. This exponent should be insensitive to the measure of weight used for the calculation (e.g. dry versus ash free, with or without shell) if the ratio between measures of weight is constant (Ricciardi and Bourget, 1998). It should also be insensitive to whether *C* or *Q* is used if filtration efficiency is constant for a given experiment. Riisgård (2001) cited examples of several studies that reported exponents close to *b*=2/3 and *d*=2 for various species of bivalves. Meyhöfer (1985) measured pumping rates, weights and gill areas for four species of bivalves and reported exponents close to 1 for the relationship between gill area and pumping rate for three species, but more variable results for the relationships between weight and gill area and between weight and pumping rate.

To further examine scaling for *M. arenaria*, we return to the comparison of our study with two clearance-rate studies for which *E*=1 (Jørgensen and Riisgård, 1988; Riisgård and Seerup, 2003; our Fig. 7). Riisgård and Seerup (2003) reported that pumping rate scaled with shell length as $Q=7\times10^{-4}\times L^{2.47}$ for *M. arenaria*, whereas we calculated a relationship of $Q=0.067\times L^{1.0}$ for our data (not shown). Similarly, for the relationship between weight and pumping rate, Riisgaård and Seerup (2003) report $Q=4.76\times W^{0.71}$ (DW), whereas we found $Q=5.1\times W^{0.34}$ (AFDW). The discrepancies in these exponents may be due in part to an increase in pumping-rate variance for larger clams – both between individuals and between

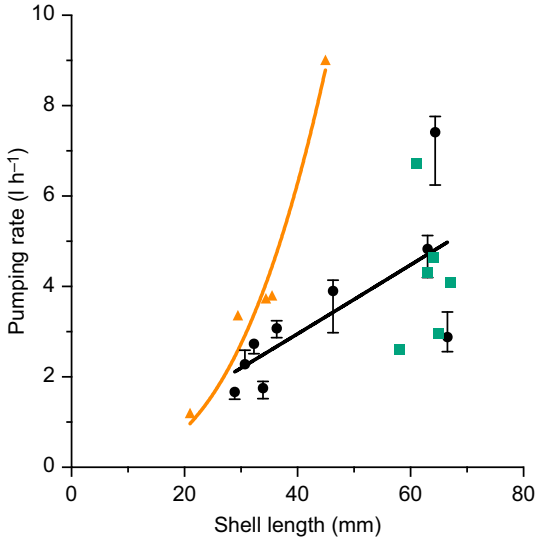

Fig. 7. Comparison of *Mya arenaria* pumping rates from this study (black circles and line; *n*=9, $y=6.7\times10^{-2}\times x^{1.0}$, $R^2=0.49$) with pumping rates from Jørgensen and Riisgård (1988; green squares; *n*=6) and Riisgård and Seerup (2003; orange triangles and line; *n*=5, $y=7\times10^{-4}\times x^{2.47}$, $R^2=0.95$).

Journal of Experimental Biology (2017) 220, 2096-2107 doi:10.1242/jeb.147934

sequences for a given individual – apparent in our data and corroborated by the results from the other two studies (Jørgensen, 1986; Riisgård and Seerup, 2003). It may also reflect the wider range of shell lengths of the clams used in our study. Our results for *M. arenaria* suggest that these exponents may be more variable than expected based on previous scaling arguments. Taking another approach to scaling, we note that:

$$Q = \overline{W}_{\text{in}} \times \frac{1}{4}\pi D_{\text{in}}^2, \quad (7)$$

for flow into the inhalant siphon. Based on our results for *M. arenaria*, we do not find a strong correlation between $\bar{W}_{\text{in}}$ and weight (Fig. 4) or shell length (not shown). If we take $\bar{W}_{\text{in}}$ to be constant, we find $Q \propto D_{\text{in}}^2$. For our experimental animals, we find that D_{in} scales with shell length as $D_{\text{in}} \propto L^{0.55}$ (Fig. 3). Inserting this back into Eqn 7, we find that $Q \propto L^{1.1}$, which is similar to our result: $Q \propto L^{1.0}$ (d=1.0). Taking D_{in} to scale linearly with L gives d=2, the relationship suggested by Riisgård and Seerup (2003). We hope that future studies will help to clarify these important scaling relationships by including more individuals over broader size ranges. It will also be important to report siphon diameters and, in particular, to correlate siphon diameters with other measures of animal size.

Capture regions

Capture region interaction times (T_{i}) suggest the magnitude of local seston depletion in still water (Fig. 6). *Mya arenaria* and *C. intestinalis* have much shorter T_{i} than *M. mercenaria* – *M. arenaria* because of its high Re_{in} and *C. intestinalis* because of its high densities. When capture regions do not overlap, each suspension feeder in a population is unaffected by the feeding activity of its neighbors. When capture regions do overlap, feeding rates are reduced by local depletion of seston. Advection of seston from outside of the population capture regions counteracts local depletion. Calculations of T_{i} for random distributions are conservative estimates for the earliest effects of local depletion. Local depletion will begin earlier in populations with patchy distributions. Based on preliminary model results (not shown), the presence of benthic boundary layer and exhalant siphon flows may lead to earlier local depletion because both stretch capture regions horizontally. Beginning at the T_{i} for uniform distributions, local depletion will be important regardless of population distribution.

Capture region extent may also have implications for olfaction because a suspension feeder can only access chemical cues within its capture region (Fig. 5). The time to respond to a chemical cue depends on the time required for the capture region to overlap the cue, so capture region growth may limit response times (Fig. 6).

Conclusions

By using CFD simulations, we were able to use the part of the flow for which we had accurate measurements to calculate Re_{in} values without relying on fits to empirical models. The advantage of this method can be demonstrated by comparing an axial profile from a CFD profile with an exponential fit (Troost et al., 2009). The effects of missing data due to laser reflection can be simulated by fitting an exponential function of the form $w=A\times e^{-Br}$ to an axial profile from a CFD simulation (D=3.0 mm, Re_{in}=300) and sequentially excluding more data in the region closest to the siphon (Fig. 8). When the function is fitted to the full profile, the approximation is fairly accurate, predicting a velocity of 110.8 mm s^{-1}, slightly higher than the true value of 109.0 mm s^{-1}. As more data are excluded from the fit, however, the prediction of the velocity at the siphon inlet quickly diverges from the true value, and excluding the 4 mm of velocity data closest to the siphon, which is realistic for a PIV experiment, yields a prediction nearly an order of magnitude lower (13.7 mm s^{-1}) at the siphon inlet. The use of CFD models allowed us to more accurately measure pumping rates and other suspension-feeding parameters and to perform capture region calculations that require the complete flow field.

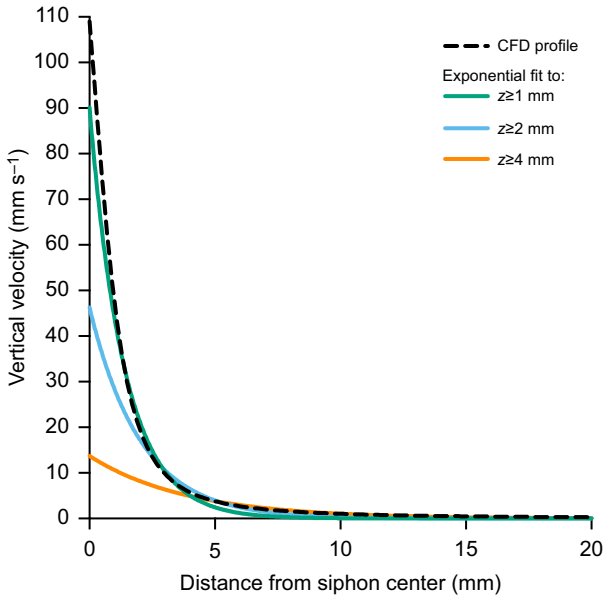

Fig. 8. An axial velocity profile from a CFD model with D=3.0 mm and Re=300 (dotted line) compared with fits to the exponential function $w=Ae^{-Br}$. Inner sections of the profile of varying length were excluded from the fit to simulate missing data near the siphon inlet. A fit to the full profile (not shown) predicts that w=110.8 mm s^{-1} at the siphon inlet (z=0), close to the true value of 109.0 mm s^{-1}. A fit excluding the 4 mm closest to the siphon, however, predicts w=13.7 mm s^{-1}, nearly an order of magnitude below the true value.

We have presented results from a new technique for quantifying suspension-feeding flows. Indirect measurement techniques are often highly dependent on experimental conditions and have complicated comparisons between studies. We hope that the use of non-invasive, direct methods, such as the one presented here, will help to reveal general patterns in suspension feeding that may be masked by experimental conditions. Experiments that combine indirect and direct methods may be especially valuable. We would also like to emphasize the utility of *Re* as a dimensionless parameter for quantifying and comparing siphon flows and the importance of reporting siphon inner diameters, which can be used to calculate inhalant and exhalant *Re* and velocities and other parameters of interest. Accurate measurements of suspension-feeding rates are crucial for ecosystem models (Cranford et al., 2011; Cerco and Noel, 2010). The wide range in published suspension-feeding rate measurements (Table 2) indicates the need for more robust methods, such as those presented here.

APPENDIX

Sensitivity analysis

A sensitivity analysis was performed by fitting profiles using the same method presented in the Results. Rather than minimizing R^2 between PIV and CFD profiles, however, we compared shifted CFD profiles with equivalent untransformed CFD profiles with a range of Re_{in}. Depending on the direction of the shift, a shifted profile was obtained either by transforming an unshifted profile or by shifting

the transect used to extract the profile from the velocity field. We compared shifted axial and radial profiles with their unshifted equivalents. The primary goals were to compare the robustness of the axial and radial profile methods and to examine overall trends in the relative effects of different types of shifts. We therefore compared a range of shifts in z direction, r direction and angle (θ) for both axial and radial profiles. To simplify comparisons, only two Re_{in} values (200 and 400) and only radial profiles taken 7 mm from the siphon inlet were tested.

Shifting axial profiles in the z direction (i.e. toward or away from the siphon) produced relatively large changes in Re_{in} values (Fig. S2A,B). The effect of shifts in the z direction was highly dependent on direction. For example, shifting the profile 0.4 mm toward the siphon (negative z direction) increased the Re_{in} value by 85 at Re_{in}=200 and 160 at Re_{in}=400, while shifting the profile 1 mm away from the siphon (positive z direction) only decreased the value by 60 and 115, respectively. Shifts in the r direction were performed in only one direction because the profiles are symmetric about the z-axis. Fits were less sensitive to shifts in the r direction than to shifts in the z direction (Fig. S2C,D). A shift of 0.4 mm increased the Re_{in} value by 35 for Re_{in}=200 and 65 for Re_{in}=400. Re_{in} calculations were fairly insensitive to angle in the 0–30 deg range, probably because the profiles themselves are very similar within that range (Fig. S2E,F). Re_{in} values differed by ≤5 from the true Re within 15 deg of the axis at Re_{in}=200 and within 11 deg of the axis at Re_{in}=400. Therefore, inaccurate measurements of siphon inlet angle are unlikely to have significant effects on Re_{in} calculations. R^2 values were fairly insensitive to all three types of shift but were most sensitive to shifts in the r direction.

Calculations of Re_{in} from radial profiles were much less sensitive than those from axial profiles to shifts in both the z and r directions. Shifting profiles toward the siphon by 0.4 mm increased Re values by 15 at Re_{in}=200 and 35 at Re=400, and shifting profiles away from the siphon by 0.4 mm decreased Re_{in} values by 15 and 30, respectively (Fig. S3A,B). Shifting profiles by 0.4 mm in the r direction increased Re_{in} values by 10 at Re_{in}=200 and 20 at Re_{in}=400 (Fig. S3C,D). Changes in siphon inlet angle produced slightly larger errors in Re_{in} calculations for radial than for axial profiles (Fig. S3E,F). An angle of 10 deg decreased the Re_{in} value by 25 at Re_{in}=200 and 50 at Re_{in}=400. R^2 values were fairly insensitive to all three types of shift but were most sensitive to shifts in angle.

When using profiles to calculate Re_{in}, accurately locating the center of the siphon is crucial to producing an accurate result. Calculations of Re_{in} from radial profiles appear to be much less sensitive overall to errors in siphon center position measurement than those from axial profiles. The higher error associated with rotation of radial profiles is unlikely to be important except at high Re_{in}, because an error of more than 10 deg is much less likely in practice than an error on the order of 0.1 mm in the r or z direction. In the case of a discrepancy in Re_{in} calculation between the two methods, the calculation from the radial profile is more likely to be accurate. Because calculations from radial profiles converge on the true Re_{in} more quickly than calculations from axial profiles when approaching the true siphon center measurement, the degree of agreement between the two calculations may be a good diagnostic for the accuracy of the siphon coordinate measurements.

Unfortunately, while R^2 appears to be a good metric for choosing the Re_{in} values, it does not appear to be a good predictor of the accuracy of siphon coordinate measurements – except in the case of very bad fits – because it is relatively insensitive to profile shifts. For calculations from radial profiles, this insensitivity may be related to the self-similar properties of the flow. A change in the distance at which a radial profile is taken may have a similar effect on the shape of the profile as a change in the mean inlet velocity.

We did not include siphon diameter D_{in} in our sensitivity analysis, but errors in measuring D_{in} may be important as well. Based on Eqn 1, errors in Re_{in} should be directly proportional to D_{in} measurement errors. We assumed that D_{in} was constant throughout the course of sequence. Although we did not formally test for this effect, D_{in} did not appear to change when the animal was pumping steadily in any of the sequences analyzed in this study. It is also worth noting that siphons are not perfectly circular in cross-section as the axisymmetric CFD models assume. The axisymmetric assumption is probably reasonable for *M. arenaria* and *C. intestinalis*, both of which had mean ratios of long to short inhalant siphon axes of 1.1, but a 3D model might produce better results for *M. mercenaria*, for which the ratio is 1.3. Fits will also be affected by additional water currents not produced by the inhalant siphon, particularly those from the exhalant jet and from thermal convection. The use of the inward component of velocity helps to mitigate the influences of these currents – particularly jet currents because they are largely unidirectional – but cannot entirely eliminate them.

Self similarity

A flow exhibits self similarity if profiles of a property – taken from different parts of the flow field – match when scaled by factors that depend on a single variable (George, 1989). For example, Pope (2000, chapter 5) describes the self similar properties of round jet flow, for which radial profiles of axial and radial velocity converge on a single curve for each velocity component, when properly scaled. Based on Pope's description, we hypothesized that inhalant siphon flows would also exhibit self-similar properties.

We compared CFD-based radial profiles of w and u centered at distances z^* from the center of the siphon entrance, where $z^*=z/D$ (Fig. S4A,B). We define $w_0=w(r=0)$ and u_0 as the maximum w and u velocities, respectively, and $r_{1/2}$ as the r-coordinate at which $w=w_0/2$. As z^* increases, w_0 and u_0 decrease, and the profiles spread ($r_{1/2}$ increases). We scale the profiles by dividing r, u and w by $r_{1/2}$, u_0 and w_0, respectively (Fig. S4B), as Pope (2000) does for a round jet. For both w and u, the scaled profiles collapse onto a single curve (i.e. they are self similar), except for the profile taken at $z^*=1$, which is within the development region. Profiles taken farther from the siphon center ($z^*>16$) collapse onto the same curves (not shown).

Acknowledgements

Carolyn Garrity assisted in early PIV experiments not included in the manuscript. Mick Devin at the Darling Marine Center provided algae. Two anonymous reviewers provide valuable feedback on the manuscript.

Competing interests

The authors declare no competing or financial interests.

Author contributions

Conceptualization: K.T.D.C., P.A.J., K.T.D.C.; Methodology: K.T.D.C., P.A.J.; Software: K.T.D.C.; Investigation: K.T.D.C., I.T.J., T.J.C.; Formal analysis: K.T.D.C., I.T.J.; Writing – original draft preparation: K.T.D.C.; Writing – review and editing: K.T.D.C., I.T.J., T.J.C., P.A.J., D.C.B.; Supervision: K.T.D.C., P.A.J.; Funding acquisition: P.A.J.

Funding

This research is part of a collaborative project (National Science Foundation grant OCE-1260232 to P.A.J., and grant OCE-1260199 to J. Crimaldi, University of Colorado). Funding was also provided by NSF grant OIA-1355457 to Maine EPSCoR at the University of Maine (D.C.B.).

Data availability

Data have been deposited in the Biological and Chemical Oceanography Data Management Office (bco-dmo.org, accession numbers 655604 and 655656).

Supplementary information

Supplementary information available online at
http://jeb.biologists.org/lookup/doi/10.1242/jeb.147934.supplemental

References

Allen, J. A. (1962). Preliminary experiments on the feeding and excretion of bivalves using *Phaeodactylum* labelled with ^{32}P. *J. Mar. Biol. Assoc. UK* **42**, 609-623.

André, C., Jonsson, P. R. and Lindegarth, M. (1993). Predation on settling bivalve larvae by benthic suspension feeders: the role of hydrodynamics and larval behavior. *Mar. Ecol. Prog. Ser.* **97**, 183-192.

Avila, K., Moxey, D., de Lozar, A., Avila, M., Barkley, D. and Hof, B. (2011). The onset of turbulence in pipe flow. *Science* **333**, 192-196.

Batchelor, G. (1967). *An Introduction to Fluid Dynamics*. Cambridge, UK: Cambridge University Press,

Caraco, N. F., Cole, J. J. and Strayer, D. L. (2006). Top down control from the bottom: regulation of eutrophication in a large river by benthic grazing. *Limnol. Oceanogr.* **51**, 664-670.

Cerco, C. F. and Noel, M. R. (2007). Can oyster restoration reverse cultural eutrophication in Chesapeake Bay? *Estuaries and Coasts* **30**, 331-343.

Cerco, C. F. and Noel, M. R. (2010). Monitoring, modeling, and management impacts of bivalve filter feeders in the oligohaline and tidal fresh regions of the Chesapeake Bay system. *Ecol. Model.* **221**, 1054-1064.

Cerrato, R. M., Caron, D. A., Lonsdale, D. J., Rose, J. M. and Schaffner, R. A. (2004). Effect of the northern quahog *Mercenaria mercenaria* on the development of blooms of the brown tide alga *Aureococcus anophagefferens*. *Mar. Ecol. Prog. Ser.* **281**, 93-108.

Clark, P. J. and Evans, F. C. (1954). Distance to nearest neighbor as a measure of spatial relationships in populations. *Ecology* **35**, 445-453.

Cloern, J. E. (1982). Does the benthos control phytoplankton biomass in South San Francisco Bay?. *Mar. Ecol. Prog. Ser.* **9**, 191-202.

Commito, J. A. (1982). Effects of *Lunatia heros* predation on the population dynamics of *Mya arenaria* and *Macoma balthica* in Maine, USA. *Mar. Biol.* **69**, 187-193.

Coughlan, J. and Ansell, A. D. (1964). A direct method for determining the pumping rate of siphonate bivalves. *ICES J. Mar. Sci.* **29**, 205-213.

Cranford, P. J., Ward, J. E. and Shumway, S. E. (2011). *Bivalve filter feeding: variability and limits of the aquaculture biofilter. In Shellfish Aquaculture and the Environment (ed. S. E. Shumway)*, pp. 81-124. Oxford: Wiley-Blackwell.

Crimaldi, J. P., Koseff, J. R. and Monismith, S. G. (2007). Structure of mass and momentum fields over a model aggregation of benthic filter feeders. *Biogeosci. Discuss.* **4**, 493-532.

Delavan, S. K. and Webster, D. R. (2012). Predator and flow influence on bivalve clam excurrent jet characteristics. *J. Exp. Mar. Biol. Ecol.* **432-433**, 1-8.

Fiala-Médioni, A. (1978). Filter-feeding ethology of benthic invertebrates (ascidians). IV. Pumping rate, filtration rate, filtration efficiency. *Mar. Biol.* **48**, 243-249.

Fields, D. M. (2010). Orientation affects the sensitivity of *Acartia tonsa* to fluid mechanical signals. *Mar. Biol.* **157**, 505-514.

Fields, D. M. and Yen, J. (1996). The escape behaviour of *Pleuromamma xiphias* in response to a quantifiable fluid mechanical disturbance. *Zooplankton* **1**, 323-340.

Fields, D. M. and Yen, J. (1997). The escape behavior of marine copepods in response to a quantifiable fluid mechanical disturbance. *J. Plankton Res.* **19**, 1289-1304.

Fields, D. M., Shema, S. D., Browman, H. I., Browne, T. Q. and Skiftesvik, A. B. (2012). Light primes the escape response of the calanoid copepod, *Calanus finmarchicus*. *PLoS ONE* **7**, e39594.

Foster-Smith, R. L. (1978). An analysis of water flow in tube-living animals. *J. Exp. Mar. Biol. Ecol.* **34**, 73-95.

Frank, D. M., Ward, J. E., Shumway, S. E., Holohan, B. A. and Gray, C. (2008). Application of particle image velocimetry to the study of suspension feeding in marine invertebrates. *Mar. Freshwater Behav. Physiol.* **41**, 1-18.

Galtsoff, P. S. (1926). New methods to measure the rate of flow produced by the gills of oyster and other molluscs. *Science* **63**, 233-234.

George, W. K. (1989). The self-preservation of turbulent flows and its relation to initial conditions and coherent structures. In *Advances in Turbulence* (ed. W. K. George and R. Arndt), pp. 81-124. New York: Hemisphere Publishing Corporation.

Goldberg, E. D., McBlair, W. and Taylor, K. M. (1951). The uptake of vanadium by tunicates. *Biol. Bull.* **101**, 84-94.

Green, S., Visser, A. W., Titelman, J. and Kiørboe, T. (2003). Escape responses of copepod nauplii in the flow field of the blue mussel, *Mytilus edulis*. *Mar. Biol.* **142**, 727-733.

Gust, G. and Harrison, J. T. (1981). Biological pumps at the sediment–water interface: mechanistic evaluation of the alpheid shrimp *Alpheus mackayi* and its irrigation pattern. *Mar. Biol.* **64**, 71-78.

Hamwi, A. and Haskin, H. H. (1969). Oxygen consumption and pumping rates in the hard clam *Mercenaria mercenaria*: a direct method. *Science* **163**, 823-824.

Jørgensen, C. B. (1986). The bivalve pump. *Mar. Ecol. Prog. Ser.* **34**, 69-77.

Jørgensen, C. B. and Riisgård, H. U. (1988). Gill pump characteristics of the soft clam *Mya arenaria*. *Marine Biology* **99**, 107-109.

Jumars, P. A. (2013). Boundary-trapped, inhalant siphon and drain flows: pipe entry revisited numerically. *Limnol. Oceanogr.* **3**, 21-39.

Karagozian, A. R. (2014). The jet in crossflow. *Phys. Fluids* **26**, 101303.

Kiørboe, T., Saiz, E. and Visser, A. (1999). Hydrodynamic signal perception in the copepod *Acartia tonsa*. *Mar. Ecol. Prog. Ser.* **179**, 97-111.

Kustin, K., Ladd, K. V., McLeod, G. C. and Toppen, D. L. (1974). Water transport rates of the tunicate *Ciona intestinalis*. *Biol. Bull.* **147**, 608-617.

Lassen, J., Kortegård, M., Riisgård, H. U., Friedrichs, M., Graf, G. and Larsen, P. S. (2006). Down-mixing of phytoplankton above filter-feeding mussels-interplay between water flow and biomixing. *Mar. Ecol. Prog. Ser.* **314**, 77-88.

Meyhöfer, E. (1985). Comparative pumping rates in suspension-feeding bivalves. *Mar. Biol.* **85**, 137-142.

Møhlenberg, F. and Riisgård, H. U. (1978). Efficiency of particle retention in 13 species of suspension feeding bivalves. *Ophelia* **17**, 239-246.

Monismith, S. G., Koseff, J. R., Thompson, J. K., O'Riordan, C. A. and Nepf, H. M. (1990). A study of model bivalve siphonal currents. *Limnol. Oceanogr.* **35**, 680-696.

Murphy, R. C. (1985). Factors affecting the distribution of the introduced bivalve, *Mercenaria mercenaria*, in a California lagoon—The importance of bioturbation. *J. Mar. Res.* **43**, 673-692.

Nayar, K. G., Sharqawy, M. H., Banchik, L. D. and Lienhard, V. J. H. (2016). Thermophysical properties of seawater: a review and new correlations that include pressure dependence. *Desalination* **387**: 1-24.

Newell, R. I. (1988). Ecological changes in Chesapeake Bay: are they the result of overharvesting the American oyster, *Crassostrea virginica*? *Understanding Estuary* **129**, 536-546.

Newell, R. I. E. and Koch, E. W. (2004). Modeling seagrass density and distribution in response to changes in turbidity stemming from bivalve filtration and seagrass sediment stabilization. *Estuaries* **27**, 793-806.

Nishizaki, M. and Ackerman, J. D. (2017). Mussels blow rings: jet behavior affects local mixing. *Limnol. Oceanogr.* **62**, 125-136.

Officer, C. B., Smayda, T. J. and Mann, R. (1982). Benthic filter feeding: a natural eutrophication control. *Mar. Ecol. Prog. Ser.* **9**, 203-210.

O'Riordan, C. A., Monismith, S. G. and Koseff, J. R. (1993). A study of concentration boundary-layer formation over a bed of model bivalves. *Limnol. Oceanogr.* **38**, 1712-1729.

O'Riordan, C. A., Monismith, S. G. and Koseff, J. R. (1995). The effect of bivalve excurrent jet dynamics on mass transfer in a benthic boundary layer. *Limnol. Oceanogr.* **40**, 330-344.

Petersen, J. K. and Riisgård, H. U. (1992). Filtration capacity of the ascidian *Ciona intestinalis* and its grazing impact in a shallow fjord. *Mar. Ecol Prog Ser* **88**, 9-17.

Petersen, J. and Svane, I. (2002). Filtration rate in seven Scandinavian ascidians: implications of the morphology of the gill sac. *Mar. Biol.* **140**, 397-402.

Pope, S. B. (2000). *Turbulent Flows*. Cambridge University Press.

Randløv, A. and Riisgård, H. U. (1979). Efficiency of particle retention and filtration rate in four species of ascidians. *Mar. Ecol. Prog. Ser* **1**, 55-59.

Reynolds, O. (1883). An experimental investigation of the circumstances which determine whether the motion of water shall be direct or sinuous, and of the law of resistance in parallel channels. *Proc. R Soc. Lond.* **35**, 84-99.

Ricciardi, A. and Bourget, E. (1998). Weight-to-weight conversion factors for marine benthic macroinvertebrates. *Mar. Ecol. Prog. Ser.* **163**, 245-251.

Riisgård, H. U. (2001). On measurement of filtration rates in bivalves: the stony road to reliable data: review and interpretation. *Mar. Ecol. Prog. Ser.* **211**, 275-291.

Riisgård, H. U. and Seerup, D. F. (2003). Filtration rates in the soft clam *Mya arenaria*: effects of temperature and body size. *Sarsia* **88**, 416-428.

Rosa, M., Ward, J. E., Holohan, B. A., Shumway, S. E. and Wikfors, G. H. (2017). Physicochemical surface properties of microalgae and their combined effects on particle selection by suspension-feeding bivalve molluscs. *J. Exp. Mar. Biol. Ecol.* **486**, 59-68.

Sharqawy, M. H., Lienhard, V. J. H. and Zubair, S. M. (2010). Thermophysical properties of seawater: a review of existing correlations and data. *Desalination Water Treat.* **16**, 354-380.

Shumway, S. E. and Cucci, T. L. (1987). The effects of the toxic dinoflagellate *Protogonyaulax tamarensis* on the feeding and behaviour of bivalve molluscs. *Aquat. Toxicol* **10**, 9-27.

Shumway, S. E., Cucci, T. L., Newell, R. C. and Yentsch, C. M. (1985). Particle selection, ingestion, and absorption in filter-feeding bivalves. *J. Exp. Mar. Biol. Ecol.* **91**, 77-92.

Stamhuis, E. J. (2006). Basics and principles of particle image velocimetry (PIV) for mapping biogenic and biologically relevant flows. *Aquat. Ecol.* **40**, 463-479.

Stamhuis, E. J., Videler, J. J., van Duren, L. and Müller, U. (2002). Applying digital particle image velocimetry to animal-generated flows: traps, hurdles and cures in mapping steady and unsteady flows in Re regimes between 10^{-2} and 10^{5}. *Exp. Fluids* **33**, 801-813.

Journal of Experimental Biology

Svane, I. (1983). Ascidian reproductive patterns related to long-term population dynamics. *Sarsia* **68**, 249-255.

Troost, K., Stamhuis, E. J., van Duren, L. A. and Wolff, W. J. (2009). Feeding current characteristics of three morphologically different bivalve suspension feeders, *Crassostrea gigas*, *Mytilus edulis* and *Cerastoderma edule*, in relation to food competition. *Mar. Biol.* **156**, 355-372.

True, A. C. and Crimaldi, J. P. (2017). Hydrodynamics of viscous inhalant flows. *Phys. Rev. E* **95**, 053107.

Wildish, D. and Kristmanson, D. (1997). *Benthic Suspension Feeders and Flow* Cambridge: Cambridge University Press.

Wilkes, J. O. (1999). *Fluid Mechanics for Chemical Engineers*. Upper Saddle River, NJ: Prentice Hall.